Received: 14 December 2020 | Revised: 23 January 2021 | Accepted: 24 January 2021

DOI: 10.1002/jccs.202000561

SPECIAL ISSUE PAPER

JOURNAL OF THE CHINESE CHEMICAL SOCIETY

Pore morphology and topology of zeolite imidazolate framework ZIF-67 revealed by small-angle X-ray scattering

Cheng-Yu Wang[1] | **Che-Min Chou**[2] | **Po-Sen Tseng**[1] | **Cheng-Si Tsao**[3,4]

[1]Department of Materials Science and Engineering, National Chiao Tung University, Hsinchu, Taiwan

[2]National Synchrotron Radiation Research Center, Hsinchu, Taiwan

[3]Institute of Nuclear Energy Research, Taoyuan, Taiwan

[4]Department of Materials Science and Engineering, National Taiwan University, Taipei, Taiwan

Correspondence
Cheng-Si Tsao, Institute of Nuclear Energy Research, Taoyuan 32546, Taiwan.
Email: cstsao@iner.gov.tw

Funding information
Ministry of Science and Technology, Grant/Award Number: MOST 108-2221-E-009-065-MY3

Abstract

The pore characterization of ZIF system using small-angle X-ray scattering (SAXS) technique is presented for the first time. The pore characterization of ZIF-67 framework structure as model system using the conventional nitrogen adsorption and SAXS methods was performed in this work. The comparison between the results obtained by two methods can provide the verification, complementary information, and error analysis to the conventional method using nitrogen atom as probe. The pore network and morphology are subjected to the topology of ZIF framework structure. The theoretical calculation of pore morphology in the unit cage of ZIF-67 structure is verified by this SAXS characterization. This SAXS study can be used as the reference of modeling pore for general ZIF systems.

KEYWORDS

nanomaterials, physical chemistry

1 | INTRODUCTION

Metal–organic frameworks (MOF)[1,2] are a class of porous crystalline materials with high specific-surface-area constructed from metal nodes coordinated with organic ligand as linker. MOFs have a wide range of applications such as energy storage/conversion,[3] gas separation,[4] catalysis,[5] biomedicine[6] carbon capture,[7] etc. The functionality diversity can be large due to the structural tunability (pore structure modification and surface functionalization) where a variety of nodes and linker can be combined to generate an indefinite number of promising materials.[8] The structural features of the hierarchically complicated MOFs can be analyzed based on the network structure (net) topology, composed of nodes and linkers, for designing new MOF structures. The diverse topology and pore structure control of MOFs through variation of linker or metal nodes exhibit drastically different catalytic activities and properties.[9] Zeolite imidazolate frameworks (ZIFs) are a unique class of MOFs, currently attracting considerable interest by their exciting potential for hydrogen storage and carbon dioxide capture.[10] Especially, tetrahedral metal centers (typically M = Zn or Co) are coordinated by the imidazolate bridging ligand (Im = C3N2H3–), forming the extended 3D open framework with zeolite type topology. Over 150 distinct ZIF structures have been synthesized.[11–13] Remarkably, ZIFs have the combining advantages: (a) the excellent chemical and thermal stability of classical zeolite traits and (b) rich topological diversity and pore size tunability of MOFs.[10–11] It is important to explore the structure of ZIF for correlating with ZIF processing and application performance.

Among the ZIFs, ZIF-67 can be particularly synthesized by a facile and environmentally friendly method. The synthesized ZIF-67 and its derivative due to the tunable pore aperture, highly stable nanostructure, and catalytic activity have attracted great interest of scientists. For the topology of ZIF-67, the metal CO^{2+} coordinating clusters playing a part in secondary building units are linked with 2-methylimidazole. ZIF-67 showed a great performance in various applications such as catalysts, gas

adsorption, molecular separation, electrode materials, etc. Moreover, the network and pore characteristics of ZIFs have significant effects on the mechanical properties.[10] The small-angle X-ray scattering (SAXS) technique is an effective and directly nondestructive tool to study the various structures, such as size, morphology, and distribution of a large number of nanoparticles in the bulk sample.[14–17] In the past time, SAXS characterization of ZIFs almost focused on the crystal growth.[18–20] There is no SAXS study investigating the pore characteristics of ZIFs. Although the pore morphology of ZIF plays an important role in the control of functionality and performance/potential of various applications, the currently used method characterizing pore structure of ZIFs is the nitrogen gas adsorption technique. N_2 adsorption analysis can determine the textural properties, such as specific surface area (SSA), pore size distribution (PSD), total pore volume, etc. According to the literature,[21] the gas sorption analysis adopted for pore characterization has several limitations: (a) diffusional hindrance of gas molecule as probe, (b) closed porosity, (c) different interaction models between gas and adsorbent molecule, and (d) different assumptions adopted for micropore (slit-like geometry) or mesopore (cylindrical geometry). The pore analysis results obtained from different models significantly differ from one another. Moreover, the determined pore size in gas adsorption is sensitive to the size of the adopted gas molecules as probe, leading to the molecular scale resolution.

In contrast, SAXS intensity is caused by the spatial electron density around the atom, providing the very high resolution. X-ray as probe has high penetration capacity, which is not affected by the closed pores. SAXS technique is able to accurately resolve the size, geometry, and spatial network of the pores at different length scales for the porous materials, demonstrating the advantages over the usual techniques.[22–24] The SAXS characterization can gain significant insight into the real pore structure and usually serves as the complementary tool regarding the conventional gas adsorption method. However, the disadvantages of scattering method are requirement of the appropriate modeling to the scattering data and the pre-knowledge of material characteristics analyzed. The SAXS pore characterization of similar highly porous systems[25,26] such as MOFs and covalent organic frameworks (COFs), as the model of interpretation could play an important role, which is still very few. The present study presents the pore characterization of ZIF-67 structure as model system using SAXS analysis for the first time. The pore characterization of ZIF-67 using the conventional nitrogen adsorption method was also performed. The comparison between the results obtained by two methods can provide the verification, complementary information, and error analysis to the conventional gas adsorption using nitrogen as probe. This SAXS study can also be used as the reference of modeling for the pore analysis of general ZIF systems. The theoretical calculation of pore morphology according to the topology of ZIF framework structure is verified by this SAXS characterization.

2 | RESULTS AND DISCUSSION

2.1 | Powder X-ray diffraction of ZIF-67 crystal

The prepared ZIF-67 as the model system here has a three-dimensional crystalline microporous structure, constructed by the ligand mIm and CO^{2+} metal clusters. Figure 1 shows the powder X-ray diffraction (PXRD) analysis of the prepared ZIF-67 nanocrystal powders, exhibiting the sharp characteristic peaks of ZIF-67, at $2\theta = 7.7°$ for (011), at $2\theta = 10.5°$ for (002), at $2\theta = 12.9°$ for (112), at $2\theta = 18.2°$ for (222), etc..[27] The measured ZIF-64 PXRD pattern is consistent with the calculated pattern of the typical ZIF-67 bulk structure with cubic crystal symmetry and unit cell parameters $a = b = c = 16.95$ Å.[11] The well-prepared ZIF-8 crystal is expected to have ordered microporous cages and network for pore characterization.

2.2 | Textural properties measured by nitrogen gas adsorption method

To understand the textural properties of the prepared ZIF-67 crystal, the N2 77 K adsorption and desorption

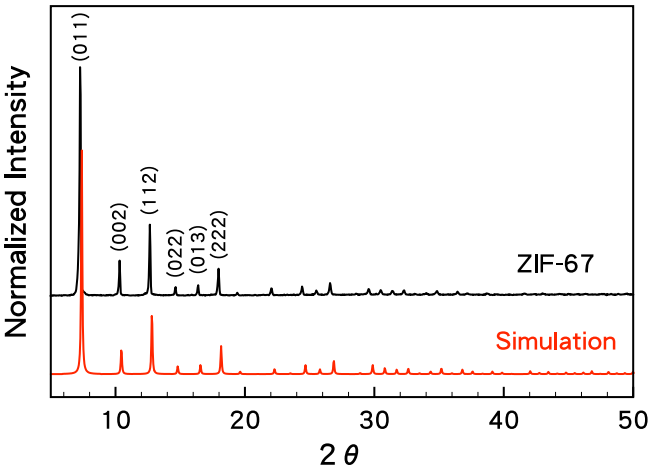

FIGURE 1 Measured PXRD pattern of ZIF-67 crystal in comparison with the theoretical calculation

measured are performed and the obtained isotherms are shown in Figure 2. The specific surface area (SEA) determined by BET method is 1780 m^2/g. Total pore volume obtained from N_2 adsorption isotherm at $P/p = 0.99$ is 0.73 cm^3/g. Micropore volume determined from t-plot model is 0.67 cm^3/g. The BET SSA of ZIF-8 is about 1780 m^2/g, which basically agrees with the literature reports[13] and is the highest among the ZIF-67 prepared by the other groups. The pore size distribution determined by nonlocal density functional theory (NLDFT) model is shown in Figure 3. The pore diameter of 1.1 nm is dominant. The pore distribution has a broad distribution ranging from 0.9 to 1.5 nm. In contrast, two peaks appeared in the pore size distribution of ZIF-8 crystal (with the same lattices structure but Zn metal cluster) determined by adsorption method and H-K model are at 1.7 and 2.2 nm.[13] Apparently, the pore size determined by gas adsorption method has a substantial discrepancy.

2.3 | Topology and framework structure

For the network topology of ZIF-67 framework structure, the metal CO^{2+} metal clusters as tetrahedral building blocks, also known as secondary building units, are coordinated by 2-methylimidazole ligand (mIm linker) into a sodalite unit cell (or called sodalite cage), as shown in Figure 4. Different architectures of the incorporated linkers (substituted ligand) cause the extended 3D open framework of ZIF structures exhibit unique network topologies (nets). SOD and LTA having cubic arrangement are two well-known types of ZIF topology,[28] as shown in Figure 4. The ZIF-7, −8, −9, and −67 structure (composition: $Zn(bIm)_2$, $Zn(mIm)_2$, $Co(bIm)_2$, and $Co(mIm)_2$, respectively) have SOD-type nets. The ZIF-20 structure has LTA-type net. The ZIF-68 (composition: Zn(bIm)(nIm)) structure has complicated GME-type net. The ZIF-8, −67, and −20 structures with cubic symmetry can afford high porosities and SSAs.[10]

2.4 | Theoretical calculation of pore in cage and open framework

According to the theoretical calculation of Yaghi's group,[29] the existence of ligand linker with a side chain

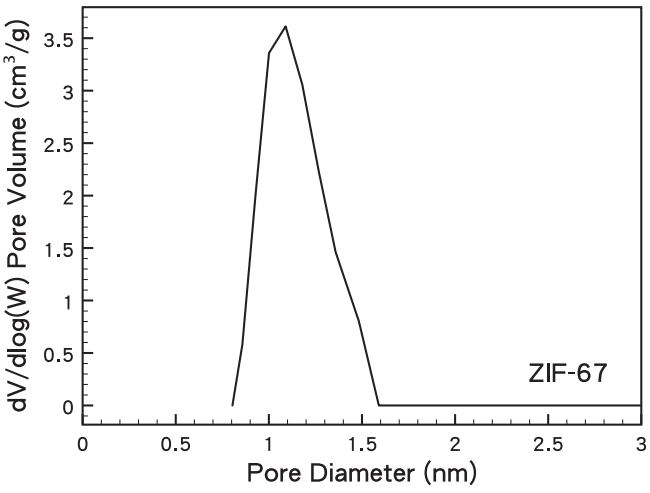

FIGURE 3 Pore size distribution determined by nitrogen gas adsorption isotherm and NLDFT model

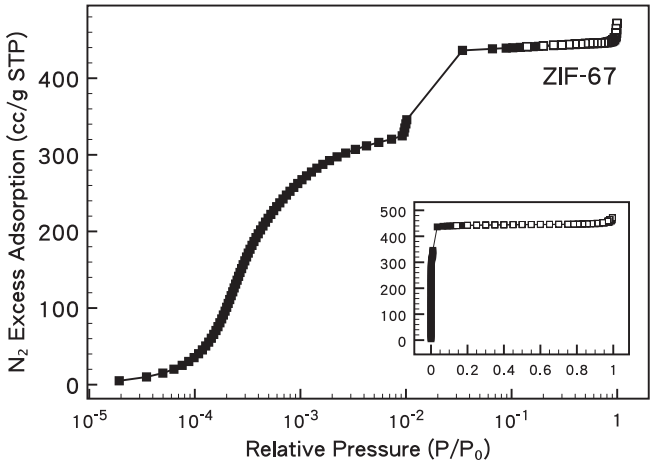

FIGURE 2 Nitrogen 77 K adsorption (solid symbol) and desorption (empty symbol; inset) isotherms of the prepared ZIF-67 crystal

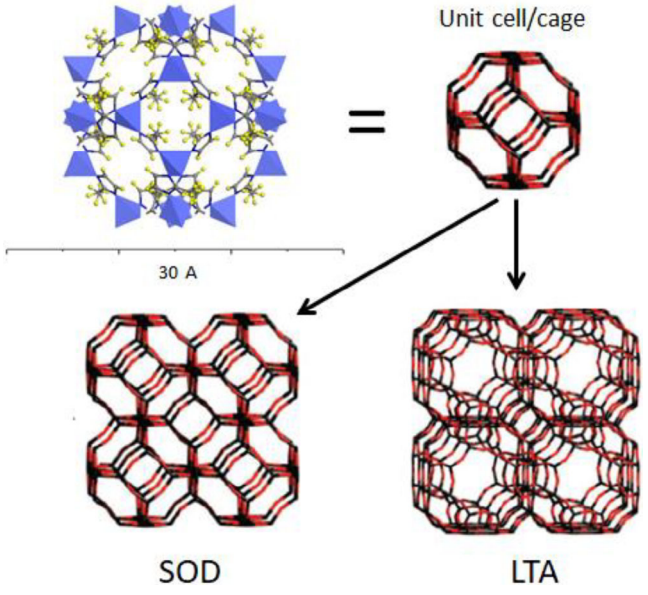

FIGURE 4 Schematic representations of (1) ZIF-67 unit cage (blue: tetrahedral metal cluster; black: carbon), and (2) SOD and LTA network topologies extended by the same unit cell/or cage

(e.g., CH_3 or NO_2 group) or an aromatic ring on the linker makes the pore heterogeneously functionalized across the series. Figure 5 shows the relationship between network topology, unit cage, and pore morphology for different ZIFs. The diameters of the largest sphere that will fit into the cavity for ZIF-8, −20, −67, and −68 structures are calculated to be 11.6, 15.4, 11.6, and 10.3 Å, respectively. On the other hand, the Cheetham's group[10] calculated the effect of pore occupancy in the ZIF-67 framework in which the DMF solvent molecules are trapped inside the pore, as shown in Figure 6. Two different calculations consistently show the diameter of accessible pore is 11.6 Å for ZIF-67.

2.5 | Pore characterization by SAXS

Figure 7 shows the measured SAXS profiles of FIZ-67 nanocrystal sample as a function of scattering vector Q. There is an upturn intensity in low-Q region of 0.01–0.12 $Å^{-1}$ showing the power-law scattering behavior ($I[Q] \propto Q$-α). Because the exponent α is 3.8, the upturn intensity can be attributed to the fractal surface of ZIF-67 crystallites. This SAXS profile has a shoulder at $Q = \sim 0.26$ $Å^{-1}$, indicating the contribution of particle form factor from spherical pores.[14,16] The SAXS profiles can be modeled by

$$I(Q) = A \cdot Q^{\alpha} + \left(\frac{4\pi}{3}\right)^2 N\Delta\rho^2 \int_0^{\infty} f(R)R^6F^2(QR)dR + b, \quad (1)$$

where the first term is used to describe the power law scattering from fractal surface of nanocrystals, A is a constant. The constant b is incoherence scattering background. The second term is the form factor of polydisperse sphere pores. N is number density of pores. Δρ is the scattering length density difference between pore and crystalline matrix. $f(R)$ is Schulz distribution and used to assume the pore size distribution. R is the pore radius. The polydispersity of pores is defined by σ/R_{avg}. σ is the variance of the size distribution. R_{avg} is the averaged radius

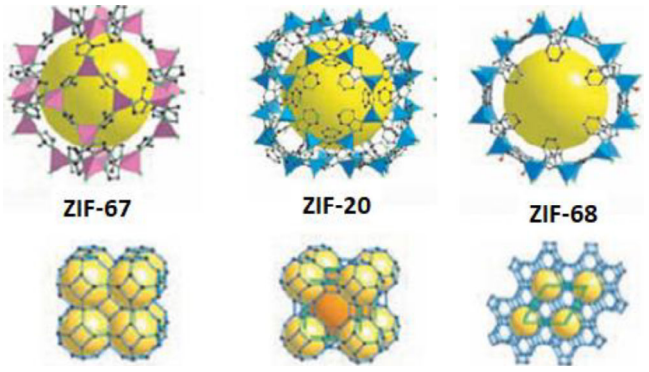

FIGURE 5 The cages of ZIF-67, −20, and −68 structures are shown in the top row (Zn tetrahedral clusters in blue; Co tetrahedral clusters in pink; linker is shown in ball-and-stick representation; C, black; N, green; O, red). The yellow ball indicates the space in the cage (corresponding pore morphology). The bottom row displays the corresponding nets (with SOD, LTA, and GME topology, respectively), demonstrating the morphology of pore network (in yellow color). Reproduced with permission from ref. [29], 2008 Copyright Science

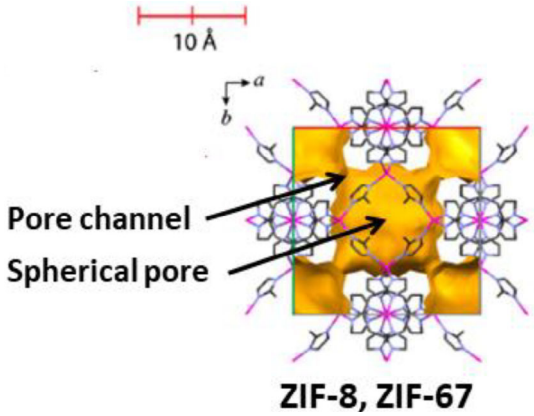

FIGURE 6 Pore morphology and accessible volumes (indicated by yellow surface) of ZIF-67 unit cage (ZIF-8 has the same cage). Hydrogen atoms are omitted here for clarity. (Zn, pink; C, gray; N, blue). (Reproduced with permission from ref. [10], 2010 Copyright, Proc. of National Academy of Science)

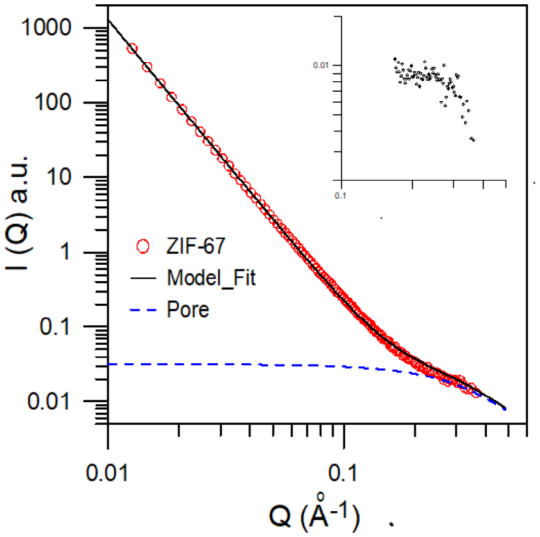

FIGURE 7 The measured SAXS profile of ZIF-67 crystal in comparison with the calculated intensity by model (solid black curve). The dashed blue line is the contribution of the form factor of spherical pores resolved from the model. The inset shows the SAXS data subtracted from the power-law-scattering data in the low-Q region and the incoherent background that is in the Q region corresponding to the pore size and have the error bars of 5–20%

of size distribution. $F(QR)$ is the scattering amplitude of the pore with radius R as given by[14,16]

$$F(QR) = \frac{[\sin(QR) - QR\cos(QR)]}{(QR)^3}. \quad (2)$$

The measured SAXS profile can be fitted well by Equation (1). The fitted diameter is 11.8 Å. The polydispersity is 13%, showing the very narrow width of distribution. This variance of pore size distribution is due to the quality at the atomic scale of the prepared ZIF-67 single crystallites. The SAXS analysis result is very close to the theoretical diameter (11.6 Å) of the pore in the cage compared to the size measured by gas adsorption method. In this work, the form factor assuming cylindrical pore cannot get the best fit result. The SAXS method using the electron density contrast can successfully probe the spherical pore morphology contained inside the unit cage.

However, The SAXS intensity contributed by the large-scale pore network formed by the all connected pores in the 3D framework structure cannot be detected due to the domination of contribution of fractal surface of crystal. On other hand, there is a diameter (3.4 Å) of a spherical pore passing through that pore (or a width of pore channel passing through the 3D framework) according to the Yaghi's crystal structure calculation.[29] The pore channel with diameter of 3.4 Å can also be seen in Figure 6. This small pore size is too small to be detected because the Q range is beyond the SAXS instrument limitation.

On the other hand, there is a model-independent approach for cross check. First of all, the Porod invariant can be calculated by the integration of SAXS profile as follows[16,25]

$$\tilde{Q} = \int_0^\infty Q^2 I(Q) dQ. \quad (3)$$

In Equation (3), $I(Q)$ is the SAXS profile subtracted from the power-law scattering intensity and the incoherent background (also shown in Figure 7). The ratio of surface to volume (S/V) for pores can be determined by Porod law as follows[16,25]

$$\frac{S}{V} = \frac{\pi}{\tilde{Q}} \left[Q^4 I(Q)\right]_{Q\to\infty}. \quad (4)$$

The $Q^4I(Q)$ value is the asymtotic value determined in the high-Q region of Porod plot. The determined S/V ratio from the SAXS profile is 0.67. The S/V ratio of spherical pore coresponding the model fitting result is 0.5 (= $3/R$). The deviation may be due to the polydispersity of pore size and the error bars of SAXS data (5–20%). In contrast, the theoretical S/V ratio of thin-rod-like pore or the pore channel formed by the confinement of network is 0.33. This value largely deviates from the result of model-independent SAXS approach. Most space of the pore channel with a diameter of 3.4 Å (indicated in Figure 6) is included in the spherical pores except for a small portion (neck connecting two spherical pores). Therefore, the SAXS intensity contributed by the small pore channel can be neglected.

3 | EXPERIMENTAL

3.1 | Synthesis of ZIF-67

The ZIF-67 was synthesized based on a previous reported literature.[27] $CO(NO_3)^2{\cdot}6H_2O$ of 1.46 and 2.46 g of 2-methylimidazole were dissolved in 75 ml of methanol followed by 30-min stirring in ambient temperature. Then, the solution aged for 24 hr at ambient temperature. The purple precipitates were filtered and washed with methanol three times. Finally, the ZIF-67 as-synthesized was evacuated in vacuum with 100°C for 12 hr.

3.2 | X-ray diffraction, nitrogen adsorption isotherms and small-angle X-ray scattering measurement

The PXRD measurement of ZIF-67 is performed by Bruker D2 Phaser X-ray diffractometer using Cu Kα (λ = 1.54 Å) target under operation of 30 kV and 10 mA. The PXRD patterns were collected from 5°–70°, with a scan step size of 0.04° and a scan rate of 7°/min. The nitrogen adsorption and desorption isotherms of ZIF-67 were obtained at 77 K using Micromeritics ASAP 2020 volumetric gas adsorption analyzer. The prepared sample was pretreated at 120°C overnight under high vacuum (<10–2 mbar) environments before nitrogen introduction. The SAXS experiment was carried out at BL23 beamline of National Synchrotron Radiation Research Center, Taiwan. The prepared SAXS sample has transmission of ~0.46. The SAXS configuration can enable the Q range be 0.007–0.4 $Å^{-1}$. The SAXS profile was reduced from 2D SAXS pattern according to the standard procedure.

4 | CONCLUSIONS

The SAXS characterization for pore morphology of ZIF stricture is presented for the first time, verifying the calculation based on the crystal structure. Pore morphology in the unit cage of ZIF-67 can be quantitatively

determined by the SAXS analysis in this work, being more effective than the conventional method. The pore network and morphology is subjected to the topology of ZIF framework structure. The NLDFT model determining the pore size distribution of ZIF based on nitrogen adsorption can provide a better evaluation than the HK model.

ACKNOWLEDGMENT

This work is supported by the Ministry of Science and Technology, Taiwan; Award MOST 108-2221-E-009-065-MY3.

ORCID

Cheng-Si Tsao https://orcid.org/0000-0003-0867-3843

REFERENCES

[1] H. Li, M. Eddaoudi, M. O'Keeffe, O. M. Yaghi, *Nature* **1999**, *402*, 276.
[2] J. R. Long, O. M. Yaghi, *Chem. Soc. Rev.* **2009**, *38*, 1213.
[3] D. Wu, Z. Guo, X. Yin, Q. Pang, B. Tu, L. Zhang, Y. G. Wang, Q. Li, *Adv. Mater.* **2014**, *26*, 3258.
[4] X. Zhang, Y. Liu, S. Li, L. Kong, H. Liu, Y. Li, W. Han, K. L. Yeung, W. Zhu, W. Yang, J. Qiu, *Chem. Mater.* **2014**, *26*, 1975.
[5] C. Wang, J. Tuninetti, Z. Wang, C. Zhang, R. Ciganda, L. Salmon, S. Moya, J. Ruiz, D. Astruc, *J. Am. Chem. Soc.* **2017**, *139*, 11610.
[6] K. Liang, R. Ricco, C. M. Doherty, M. J. Styles, S. Bell, N. Kirby, S. Mudie, D. Haylock, A. J. Hill, C. J. Doonan, P. Falcaro, *Nat. Commun.* **2015**, *6*, 7240.
[7] K. Sumida, D. L. Rogow, J. A. Mason, T. M. McDonald, E. D. Bloch, Z. R. Herm, T. H. Bae, J. R. Long, *Chem. Rev.* **2012**, *112*, 724.
[8] A. Bětard, R. A. Fischer, *Chem. Rev.* **2012**, *112*, 1055.
[9] J. Lyu, X. Zhang, K. I. Otake, X. Wang, P. Li, Z. Li, Z. Chen, Y. Zhang, M. C. Wasson, Y. Yang, P. Bai, X. Guo, T. Islamoglu, O. K. Farha, *Chem. Sci.* **2019**, *10*, 1186.
[10] J. Chong Tan, T. D. Bennett, A. K. Cheetham, *Proc. Natl Acad. Sci.* **2010**, *107*, 9938.
[11] G. Zhong, D. Liu, J. Zhang, *J. Mater. Chem. A* **2018**, *6*, 1887.
[12] C.-W. Chang, Z.-J. Gong, N.-C. Huang, C.-Y. Wang, W.-Y. Yu, *Catal. Today* **2020**, *351*, 21.
[13] C.-W. Chang, Y.-H. Kao, P.-H. Shen, P.-C. Kang, C.-Y. Wang, *J. Hazard. Mater.* **2020**, *400*, 122974.
[14] H.-C. Liao, C.-S. Tsao, T.-H. Lin, C.-M. Chuang, C.-Y. Chen, U.-S. Jeng, C.-H. Su, Y.-F. Chen, W.-F. Su, *J. Am. Chem. Soc.* **2011**, *133*, 13064.
[15] H.-C. Liao, C.-S. Tsao, T.-H. Lin, M.-H. Jao, C.-M. Chuang, S.-Y. Chang, Y.-C. Huang, Y.-T. Shao, C.-Y. Chen, C.-J. Su, U.-S. Jeng, Y.-F. Chen, W.-F. Su, *ACS Nano* **2012**, *6*, 1657.
[16] O. Glatter, O. Kratky, *Small-Angle X-Ray Scattering*, Academic Press, London **1982**.
[17] C. Chien, C.-S. Tsao, S.-K. Wu, C.-Y. Chang, P.-C. Chang, Y.-K. Kuo, *Acta Mater.* **2016**, *120*, 159.
[18] G. M. Segovia, J. S. Tuninetti, S. Moya, A. S. Picco, M. R. Ceolín, O. Azzaroni, M. Rafti, *Mater. Today Chem.* **2018**, *8*, 29.
[19] J. Cravillon, C. A. Schrçder, R. Nayuk, J. Gummel, K. Huber, M. Wiebcke, *Angew. Chem. Int. Ed.* **2011**, *50*, 8067.
[20] M. Goesten, E. Stavitski, E. A. Pidko, C. Gücüyener, B. Boshuizen, S. N. Ehrlich, E. J. M. Hensen, F. Kapteijn, J. Gascon, *Chem. Eur. J.* **2013**, *19*, 7809.
[21] C.-S. Tsao, C.-Y. Chen, T.-Y. Chung, C.-J. Su, C.-H. Su, H.-L. Chen, U.-S. Jeng, M.-S. Yu, P.-Y. Liao, K.-F. Lin, Y.-R. Tzeng, *J. Phys. Chem. C* **2010**, *114*, 7014.
[22] P. J. Hall, S. Brown, J. Fernandez, J. M. Calo, *Carbon* **2000**, *38*, 1257.
[23] V. Bock, A. Emmerling, R. Saliger, J. Fricke, *J. Porous Mater.* **1997**, *4*, 287.
[24] B. Smarsly, C. Göltner, M. Antonietti, W. Ruland, E. Hoinkis, *J. Phys. Chem. B* **2001**, *105*, 831.
[25] C.-S. Tsao, M.-S. Yu, T.-Y. Chung, H.-C. Wu, C.-Y. Wang, K.-S. Chang, H.-L. Chen, *J. Am. Chem. Soc.* **2007**, *129*, 15997.
[26] R. A. Maia, L. S. A. Carneiro, J. M. C. Cifuentes, C. D. Buarque, P. M. Estevesa, A. M. Percebom, *J. Appl. Cryst.* **2020**, *53*, 1376.
[27] S. L. Zacho, J. Mielby, S. Kegnæs, *Catal. Sci. Technol.* **2018**, *8*, 4741.
[28] L. Vilà-Nadal, L. Cronin, *Nat. Rev. Mater.* **2017**, *2*, 17054.
[29] R. Banerjee, A. Phan, B. Wang, C. Knobler, H. Furukawa, M. O'Keeffe, O. M. Yaghi, *Science* **2008**, *319*, 939.

AUTHOR BIOGRAPHIES

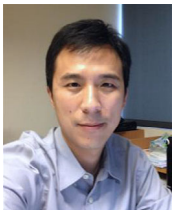

Cheng-Yu Wang is an Associate Professor at the Department of Materials Science and Engineering of the National Chiao Tung University, Taiwan. He received his PhD in the Department of Energy and Mineral Engineering at the Pennsylvania State University, USA, in 2014. He mainly studies metal–organic frameworks (MOFs) and its derivatives for hydrogen storage, hydride dehydrogenation, CO_2 capture and utilization, and photocatalysis.

Che-Min Chou is an assistant research scientisit at National Synchrotron Radiation Research Center, Taiwan. He received his PhD degree in Department of Materials Science and Engineering in 2004. His research and interests are focused on (a) Small-angle X-ray and light scattering techniques, (b) Soft matters, (c) Phase separation, (d) Industrial application of polymers.

Po-Sen Tseng obtained the bachelor's degree from Department of Materials Science and Engineering, National Chiao Tung University in 2020. His research focuses on (a) porous materials, (b) hydrogen storage and production, (c) metal–organic-frameworks, and (d) nanomaterials.

Cheng-Si Tsao is a researcher and project leader at Institute of Nuclear Energy Research, Taiwan. He is also an adjunct associate professor of Department of Materials Science and Engineering, National Taiwan University. He received his PhD degree in Department of Engineering System and Science from National Tsing-Hua University in 1999. His research and interests are focused on (a) Small-angle neutron and X-ray scattering techniques, (b) Nanomaterials, (c) Energy materials and devices, (d)Alloy, (e) Polymer, (f) Nuclear Fuel and Materials.

How to cite this article: Wang C-Y, Chou C-M, Tseng P-S, Tsao C-S. Pore morphology and topology of zeolite imidazolate framework ZIF-67 revealed by small-angle X-ray scattering. *J Chin Chem Soc*. 2021;68:500–506. https://doi.org/10.1002/jccs.202000561